View metadata, citation and similar papers at core.ac.uk

brought to you by CORE

provided by CiteSeerX

This document was prepared in conjunction with work accomplished under Contract No. DE-AC09-96SR18500 with the U. S. Department of Energy.

DISCLAIMER

This report was prepared as an account of work sponsored by an agency of the United States Government. Neither the United States Government nor any agency thereof, nor any of their employees, makes any warranty, express or implied, or assumes any legal liability or responsibility for the accuracy, completeness, or usefulness of any information, apparatus, product or process disclosed, or represents that its use would not infringe privately owned rights. Reference herein to any specific commercial product, process or service by trade name, trademark, manufacturer, or otherwise does not necessarily constitute or imply its endorsement, recommendation, or favoring by the United States Government or any agency thereof. The views and opinions of authors expressed herein do not necessarily state or reflect those of the United States Government or any agency thereof.

This report has been reproduced directly from the best available copy.

Available for sale to the public, in paper, from: U.S. Department of Commerce, National Technical Information Service, 5285 Port Royal Road, Springfield, VA 22161,
phone: (800) 553-6847,
fax: (703) 605-6900
email: orders@ntis.fedworld.gov
online ordering: http://www.ntis.gov/help/index.asp

Available electronically at http://www.osti.gov/bridge
Available for a processing fee to U.S. Department of Energy and its contractors, in paper, from: U.S. Department of Energy, Office of Scientific and Technical Information, P.O. Box 62, Oak Ridge, TN 37831-0062,
phone: (865)576-8401,
fax: (865)576-5728
email: reports@adonis.osti.gov

THE NON-CONSTANT CTOD/CTOA IN CRACK PROPAGATION

P.-S. Lam[a] , Y. Kim[b], and Y. J. Chao[b,*]

[a]Savannah River National Laboratory, Aiken, SC 29808
[b]Department of Mechanical Engineering, University of South Carolina, Columbia, SC 29208
[*]Corresponding author

Abstract

Unlike the common belief that crack propagation behavior can be predicted successfully by employing fracture criteria based on a constant crack tip opening displacement or angle (CTOD/CTOA), this paper shows that the initially non-constant portion of the CTOD/CTOA plays an essential role in predicting the fracture load for a growing crack. Three- and two-dimensional finite element analyses indicate that a severe underestimate of the experimental load vs. crack extension curve would occur if a constant CTOD/CTOA criterion is used. However, the use of a simplified, bilinear CTOD/CTOA criterion including its non-constant portion will closely duplicate the test data. Furthermore, as a result of using the experimental data from J-integral test with various crack length to specimen width ratios (a/W), it is demonstrated that the CTOD/CTOA is crack tip constraint dependent. The initially higher values of the CTOD/CTOA are in fact a natural consequence of crack growth process which is reflected by the J-resistance (J-R) curve and its slope (tearing modulus).

1. Introduction

In addition to using fracture criteria based on the stress intensity factor or J-integral, attention has recently been focused on the directly measurable quantities such as the crack tip opening displacement and/or angle (CTOD/CTOA). In this paper, the CTOD is defined as the crack opening displacement (δ) measured at a fixed distance (x) behind the current crack tip, and CTOA= $2\tan^{-1}[\delta/(2x)]$. The advance in measurement technologies allows these fracture parameters be measured accurately by means of optical microscopy (e.g., [1]), digital image correlation (e.g., [2,3]) and microtopography [4], etc. On the other hand, the development in high speed computational hardware and software leads to realistic computer simulation of fracture testing to extract these quantities at any length scale and in three-dimensional space. The combination of experimental and numerical results provides insight to the true fracture mechanisms in materials. A collection of recent research papers on CTOD/CTOA has been compiled by Newman and Zerbst [5].

A comprehensive review of the work on CTOD/CTOA has been provided by Newman, et al. [6]. The majority of the test data (e.g., aluminum alloys and A533B) and the numerical analyses (e.g., [1,7-20]) seem to indicate that the values of CTOD/CTOA are initially high, but progressively decrease to a nearly constant value after several millimeters of crack growth. It has been shown by several investigators (e.g., [10,11,12,16,21-24]) that, based on three-dimensional (3D) and two-dimensional (2D) finite element analyses, a constant CTOD/CTOA fracture criterion may be capable of predicting the experimental data (e.g., load versus crack extension curves). This leads to

a speculation that the initially higher values of CTOD/CTOA may be a result of inadequate measurement on the specimen surface; while crack tunneling, shear lips or slant fracture may have occurred during the test in specimens including compact tension (CT) and middle-cracked tension (MT).

The assumption of a constant CTOD/CTOA fracture criterion is consistent with the intent of earlier analyses on Mode I crack growth under small scale yielding (SSY) [25-30] and general yielding [28], in which the crack maintains a constant profile when a steady state is reached. In the finite element analyses of a growing crack under SSY [26,28-30], a relationship was established between K_{ss} and a normalized CTOA, where K_{ss} is the far field stress intensity level for steady state crack growth. In the case of general yielding, a compact tension test [31] was modeled by a finite element analysis [28]. The calculated result showed that a relatively constant CTOA seemed to exist when $\Delta a < 5$ mm (about 4.5 degrees at 0.4 mm behind the moving crack tip, or about 3.5 degrees at 0.8 mm behind the crack tip). The initial crack length of this specimen was 40.38 mm with a/W=0.8. The test material was Al-Si killed AISI 4140 steel with a nominal tensile yield strength of 1173 MPa and ultimate strength 1327 MPa, while the analysis used the elastic-perfectly plastic material idealization, with yield stress at 1173 MPa and the Young's modulus was 200 GPa. Note that in the previous studies on steady state crack growth under SSY, no attempt was made to predict the fracture load with a constant CTOD/CTOA fracture criterion, because the crack initiation was not considered and the crack growth was under J-control and was always self-similar.

In this paper, the test data from a set of single edge-notched bend (SENB) specimens are used to investigate the CTOD/CTOA during crack growth. This set of tests was previously performed for developing a constraint-modified J-R curve [32] for A285 Grade C carbon steel, based on the J-A_2 two-parameter constraint theory of fracture for elastic-plastic materials [33-35]. The specimens were side-grooved to suppress the shear lips and the fractography showed evidence of straight crack fronts. A three-dimensional finite element analysis (3D-FEA) was first carried out to simulate the crack growth according to the experimental crack length vs. load-point displacement curve of the specimen with a/W=0.59. Based on the straight crack front from the post-test fracture surface analysis, the crack front nodes in the finite element model are released simultaneously. The CTOD/CTOA can then be estimated along the crack front. A subsequent plane strain two-dimensional finite element analysis (2D-FEA) shows that the CTOD/CTOA values from both analyses are equivalent. Thus the adequacy of the 2D-FEA is established and used thereafter.

The finite element procedure is reversed to validate if the CTOD/CTOA just determined from the aforementioned 2D-FEA can indeed predict the experimental J-R curve and the load-displacement curve for the same specimen (a/W=0.59). A constant CTOD/CTOA criterion is first employed but the result shows a severe under-estimation of both of the J-R and the load-displacement curves. However, using a bilinear form of CTOD/CTOA to account for its initially higher values, a very good agreement between the experimental and predicted curves is achieved. This implies that the initial values of CTOD/CTOA contain the essential information and momentum to drive the crack to a steady state which then can be characterized by a constant CTOD/CTOA growth criterion.

The importance of the initial values of CTOA on predicting crack growth has been recognized by Kanninen et al [36] and is discussed in Kanninen and Popelar (Fig. 5.58 in

[37]). They also discovered that the use of a constant CTOA as the fracture criterion would underestimate the fracture load. Using the experimental J-R curves in Lam et al. [32] and following the derivations in Kanninen and Popelar [37] and in Gullerud et al. [17], the CTOA can be expressed as a function of the slope of the J-R curve (dJ/da) or the tearing modulus. The prediction can then be compared with the CTOA that are directly calculated from the finite element method using nodal release technique. It is shown in this paper that the initially higher values of CTOD/CTOA are a natural consequence of the crack growth resistance in a material (J-R curve), and therefore, it can be concluded that CTOD and CTOA are essentially functions of crack tip constraint.

2. Experiments

A set of single edge-notched bend (SENB) specimens was designed based on American Society for Testing and Materials (ASTM) Standard Test Method for Measurement of Fracture Toughness (E 1820) specifications, except for the initial crack lengths that were varied to achieve different levels of crack tip constraint. These specimens were originally used to develop a constraint-modified J-R curve for A285 carbon steel storage tanks [32]. The same set of test data are used in the current study of CTOD/CTOA during the course of crack extension.

The specimens were machined from A285 carbon steel Grade C, heat E400 plate with 0.18 wt.% carbon, 0.43 wt.% manganese, and 0.026 wt.% sulfur. The tensile test shows that the 0.2% offset yield stress (σ_o) is 251 MPa (36.4 ksi), the ultimate tensile stress 415 MPa (60.2 ksi), the flow stress (σ_f) 333 MPa (48.3 ksi, defined as the average of the 0.2% yield stress and the ultimate stress), and the Young's modulus (E) 207 GPa (30,000 ksi). The Poisson ratio of the material is 0.3. The true stress-true strain curve is shown in Figure 1.

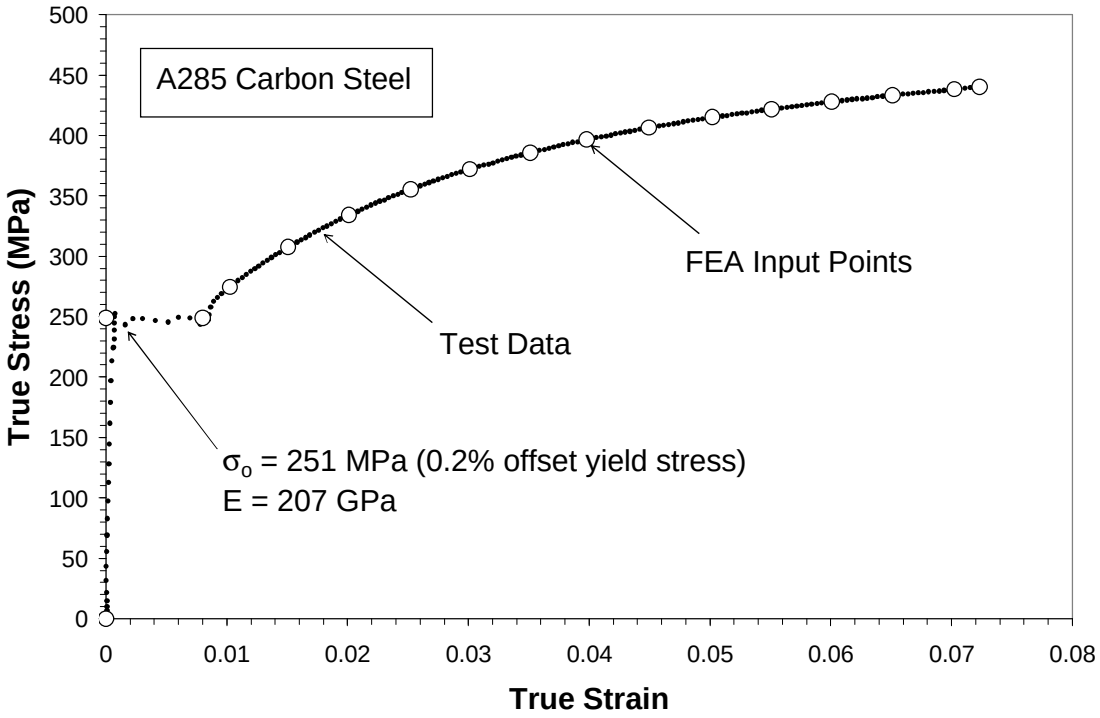

Figure 1 True stress-true strain curve for A285 Grade C heat 400 plate.

The specimen thickness B is 15.875 mm (0.625 inches) with 10% side groove on each side (net thickness is 12.7 mm or 0.5 inches), the width W is 31.75 mm (1.25 inches), the length L is 142.88 mm (5.625 inches), and the span S is 127 mm (5 inches). After fatigue cracking, the initial crack depth to the width ratios (a/W) for the fracture toughness test specimens are, respectively, 0.32 (Specimen 1D), 0.35 (Specimen 2C), 0.59 (Specimen 2A), and 0.71 (Specimen 4C).

The SENB fracture toughness testing was conducted according to the guidelines provided by ASTM E1820. Due to the large deformation occurred during testing, the crack opening mouth clip gauge was not used. However, the load and the load-point displacement are available for data analysis. The crack lengths were measured by potential drop technique and were correlated with the actual measurements on the fracture surfaces of the specimens (e.g., Fig. 2). Note that a slightly reversed thumbnail crack front was formed because of the presence of side grooves. The experimental J-R data are plotted in Figure 3, which clearly shows a distinct specimen size-dependent, in-plane constrain effect. It is intended in this paper to demonstrate that the crack tip constraint also influences the CTOD/CTOA during crack growth, and therefore any fracture criteria based on CTOD/CTOA.

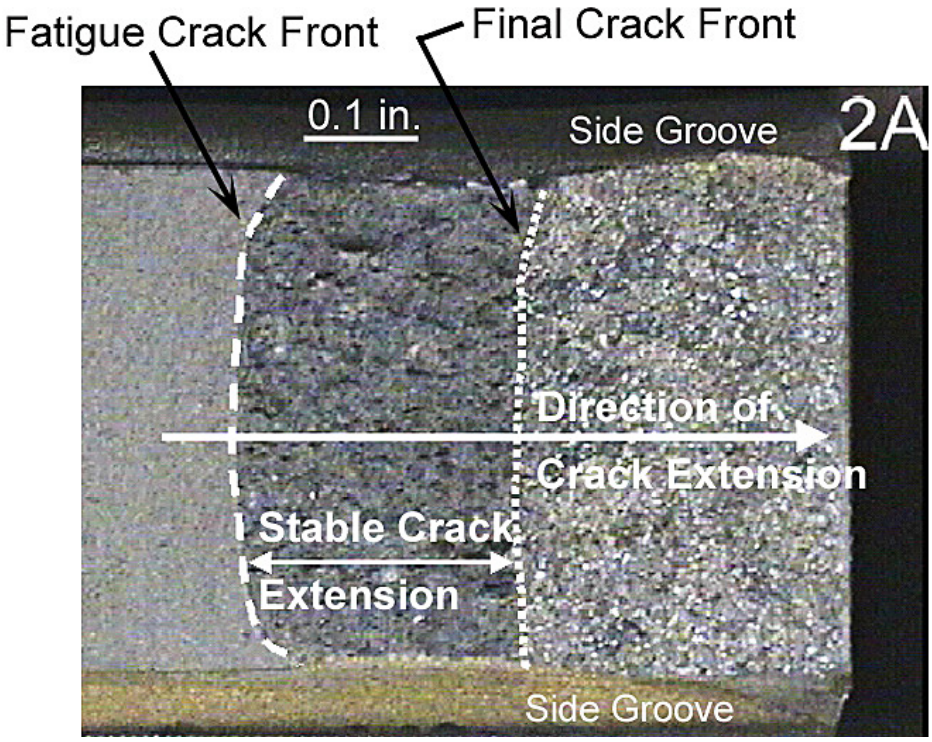

Fig.2 Typical fracture surface of the SENB Specimens.

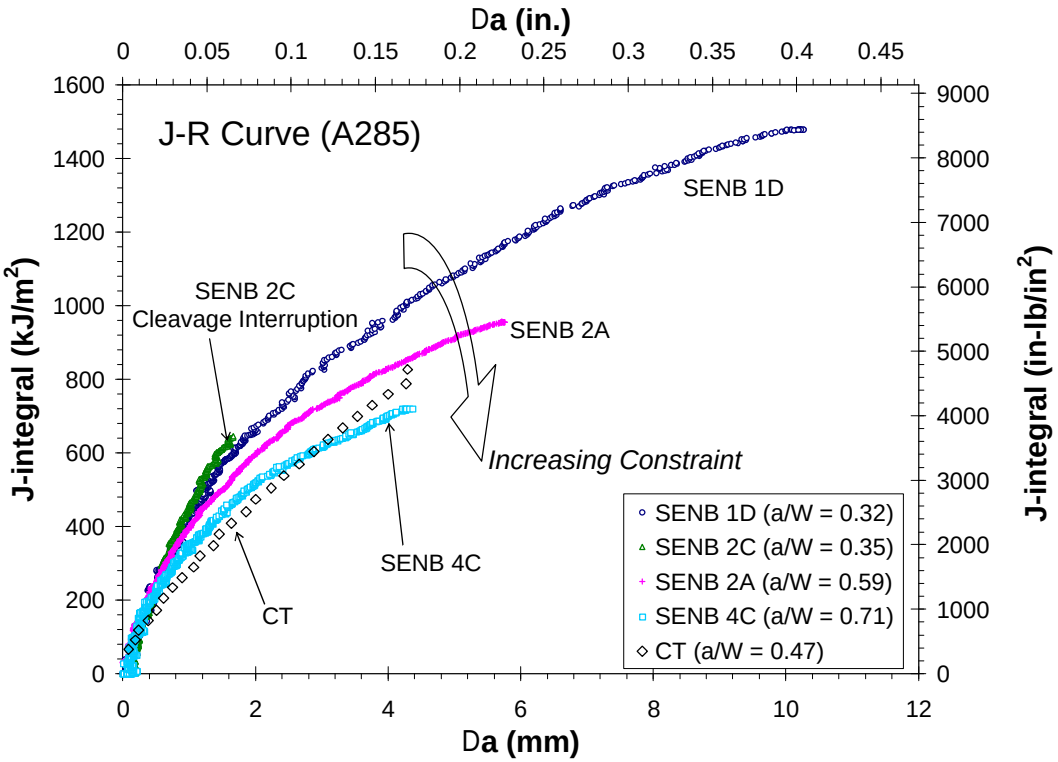

Figure 3 Experimental J-R curves with in-plane crack tip constraint.

For completeness, Figure 3 contains a J-R curve which was subject to cleavage interruption after 1.6 mm of crack extension. In addition, a J-R curve using standard CT specimen is also included. This CT specimen was cut from the same steel plate as the SENB specimens to ensure that identical material source was used and the only difference is the test specimen design. The width of the CT specimen is 63.58 mm (2.50 inches) and the a/W ratio is 0.47. The specimen height is 48.87 mm (1.92 inches) and its thickness is identical to that of the SENB specimens, that is, 15.875 mm (0.625 inches) with 10% side groove on each side.

3. Three-Dimensional Finite Element Analysis of Crack Extension

Three-dimensional finite element analysis is performed to simulate the J-integral testing. Specimen No. 2A (a/W= 0.59) was selected for the analysis. Because of symmetry, only one quarter of the SENB specimen is modeled. This model contains a 10% side groove and uses 35970 eight-node, reduced integration brick elements with 41684 nodes. To facilitate the crack growth simulation, very fine and uniformly spaced elements are arranged in the crack tip region. The general purpose finite element program ABAQUS [38] is used for calculation. The elastic-plastic analysis was carried out with the full stress-strain curve input as shown in Figure 1. The incremental plasticity is assumed for the material response above the yield point, and finite deformation formulation is invoked. The loading pin movement is imposed as a prescribed nodal displacement. Only linear elastic response is allowed for the neighboring finite elements around this load application node. This treatment has been shown to have numerical advantage and to produce better results than the use of rigid surface contact element algorithm to model the loading pin movement.

Nodal release technique is used to simulate crack growth, which follows exactly the test data of crack extension vs. load point displacement curve (Fig. 4) that was obtained from testing. Based on the nearly straight crack front on the fracture surface (Fig. 2), it is not unreasonable to assume that the crack front remains straight during the course of crack extension throughout the test. As a result, the finite elements nodes immediately ahead of the current (straight) crack front nodes are released simultaneously when the crack growth criterion (Fig. 4) is met.

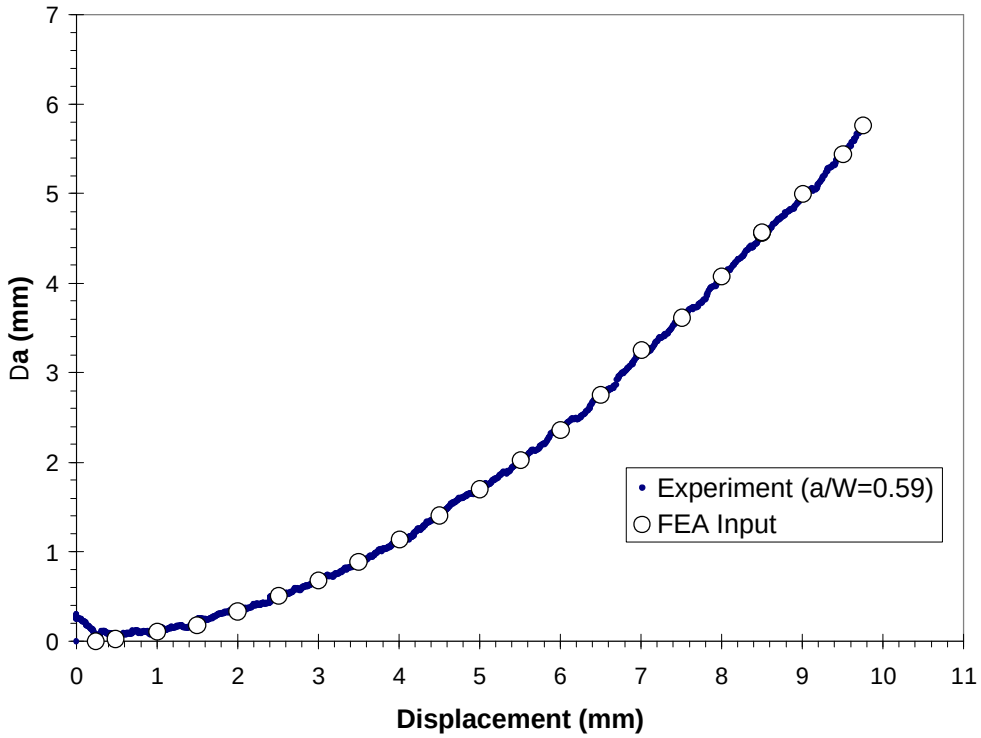

Figure 4 Crack extension test data and finite element nodal release points

The calculated load-displacement curve at the loading point is compared with the experimental curve in Figure 5. The good agreement indicates that the crack extension simulation is adequate. The CTOD and CTOA for each crack tip nodes along the crack front can be obtained from the finite element results for each increment of crack growth. In the subsequent figures, CTOA is calculated from $\mathrm{CTOA} = 2\tan^{-1}(\mathrm{CTOD}/2x)$, where x is the distance behind the current crack tip. A common choice for x is 1 mm [e.g. 6,17,39], as shown in the inset of Figure 6.

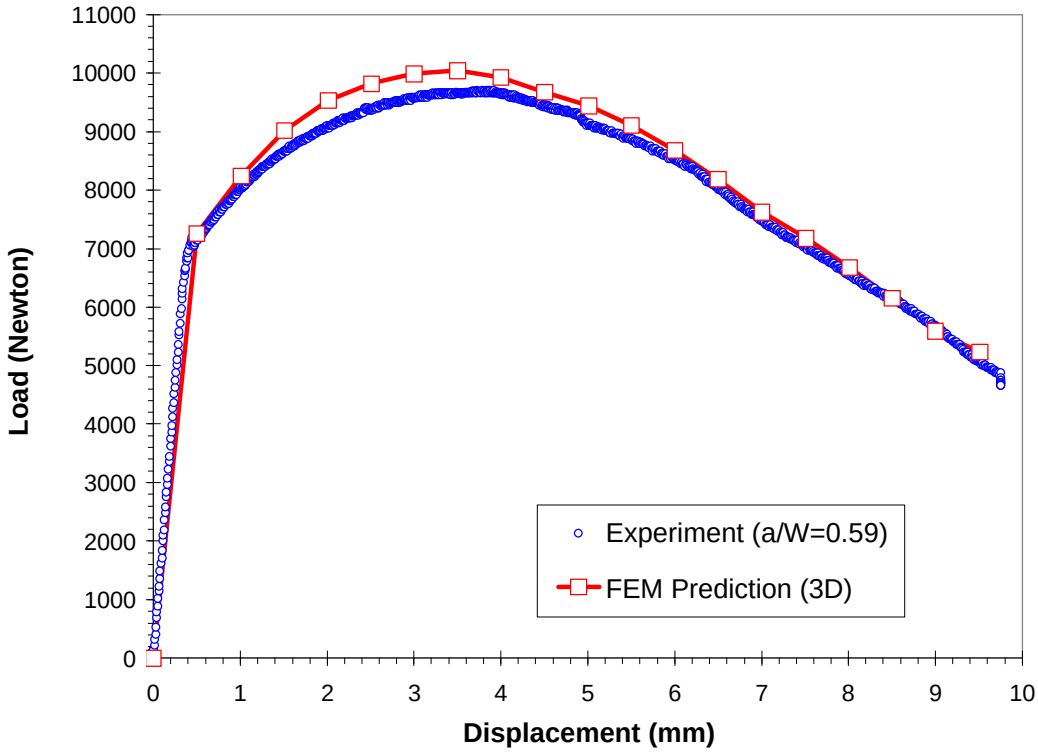

Figure 5 Comparison of predicted and experimental load-displacement curve.

Figure 6 shows the calculated CTOA of the specimen at various amount of crack growth (Δa). It can be seen that the CTOA distribution is not sensitive across the thickness t, where z=0 represents the mid-thickness of the plate, and z= 0.5t is the plane at the root of the side groove. The result of an equivalent plane strain finite element analysis is also plotted in Figure 6. The details of the 2D-FEA will be discussed in Section 4 of this paper. Because the flat crack front (Fig. 2) and the results shown in Figure 6, it may be concluded that the 2D-FEA is sufficient for this specimen type and loading condition (i.e., SENB specimens with side grooves to promote plane strain crack growth). The most significant finding in Figure 6 is that, when Δa is small the CTOA values are initially high, but progressively decrease to a nearly constant value. Note that in this experiment the fracture surface showed no evidence of tunneling. This finding may contradict a common speculation that the high CTOA values measured on the specimen surface at early stage of crack growth could be caused by the tunneling effect [6].

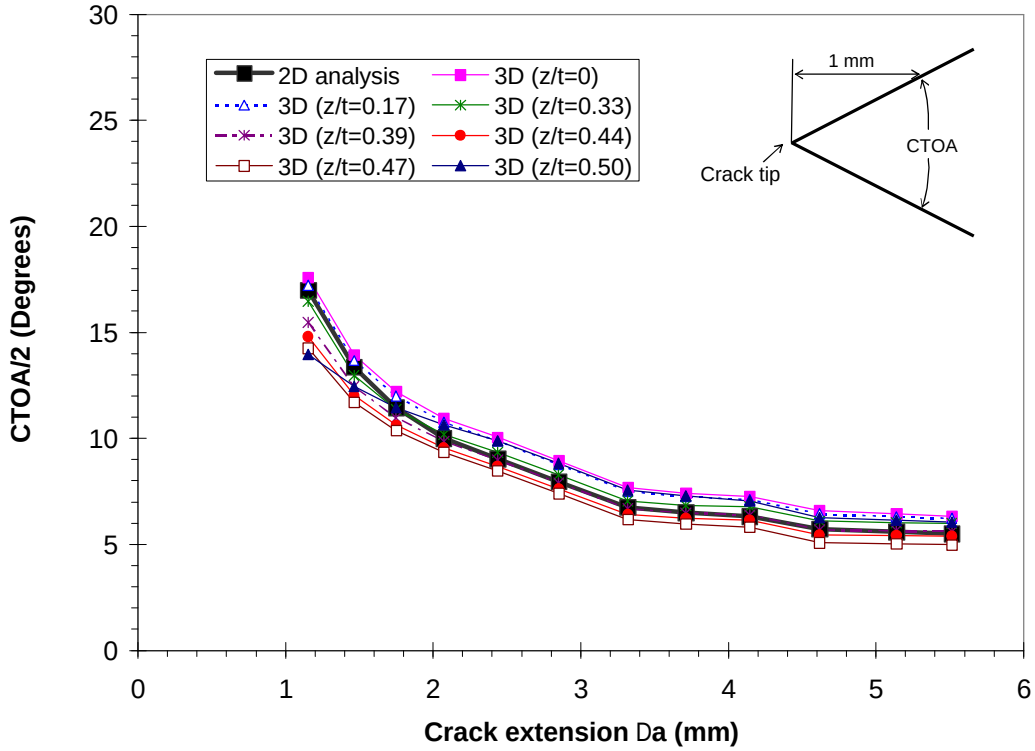

Figure 6 CTOA at 1 mm behind the crack tip vs. crack extension

The CTOA variation in the thickness direction is plotted in Figure 7. It can be seen that the CTOA is relatively uniform along the crack front through the thickness at any amount of crack growth in the test range. The CTOA values at large Δa (up to 5.5 mm) are not plotted for clarity reasons because the CTOA values converge rapidly to about 12° as Δa increases. The corresponding plane strain solutions are included as well in Figure 7 to demonstrate that the 2D-FEA is indeed appropriate for this case.

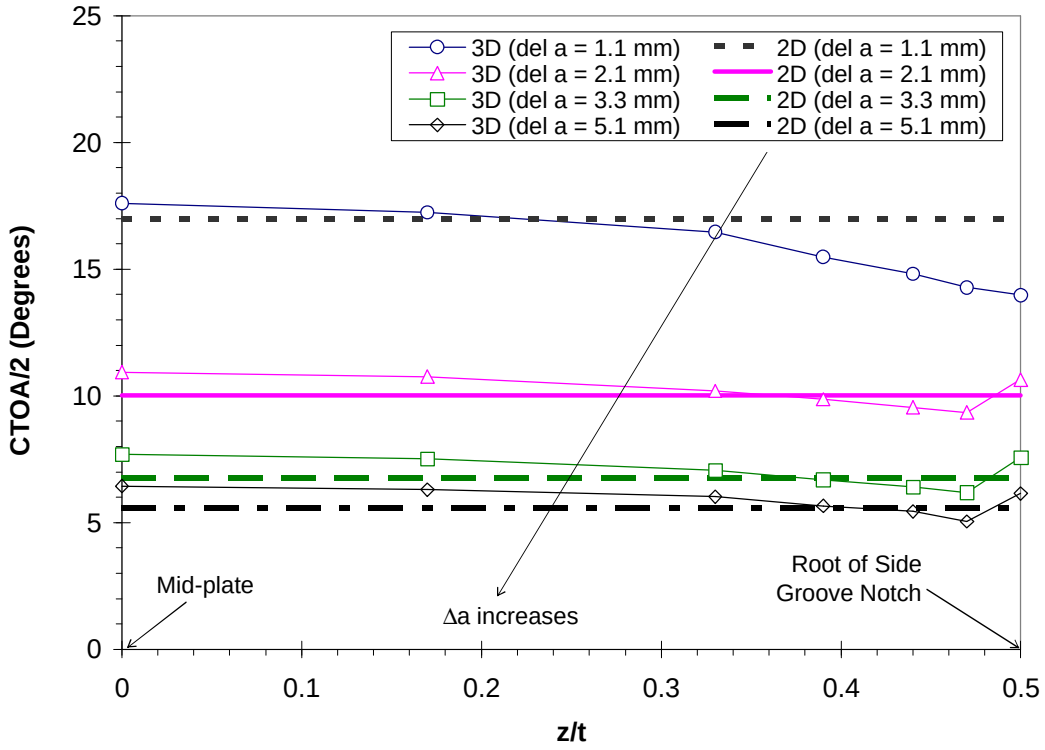

Figure 7 CTOA Distribution through the thickness (measured at 1 mm behind the current crack tip)

Figure 8 summarizes the 3D-FEA results on the crack opening profile or CTOD measured at various locations behind the current crack tip. As the crack growth continues, the CTOD progressively settles with a nearly constant profile. For any given crack extension (Δa), the value of CTOD depends on where the measurement takes place. At a specified distance from the current crack tip, this value is higher in the early crack growth phase and then decreases to a relatively constant CTOD as Δa increases. Therefore, it is important to recognize that 1) CTOD/CTOA varies with the distance behind the crack tip; 2) CTOD/CTOA varies with the amount of crack growth (Δa); and 3) CTOD/CTOA fracture criteria should be reported and used with a specified distance from the crack tip.

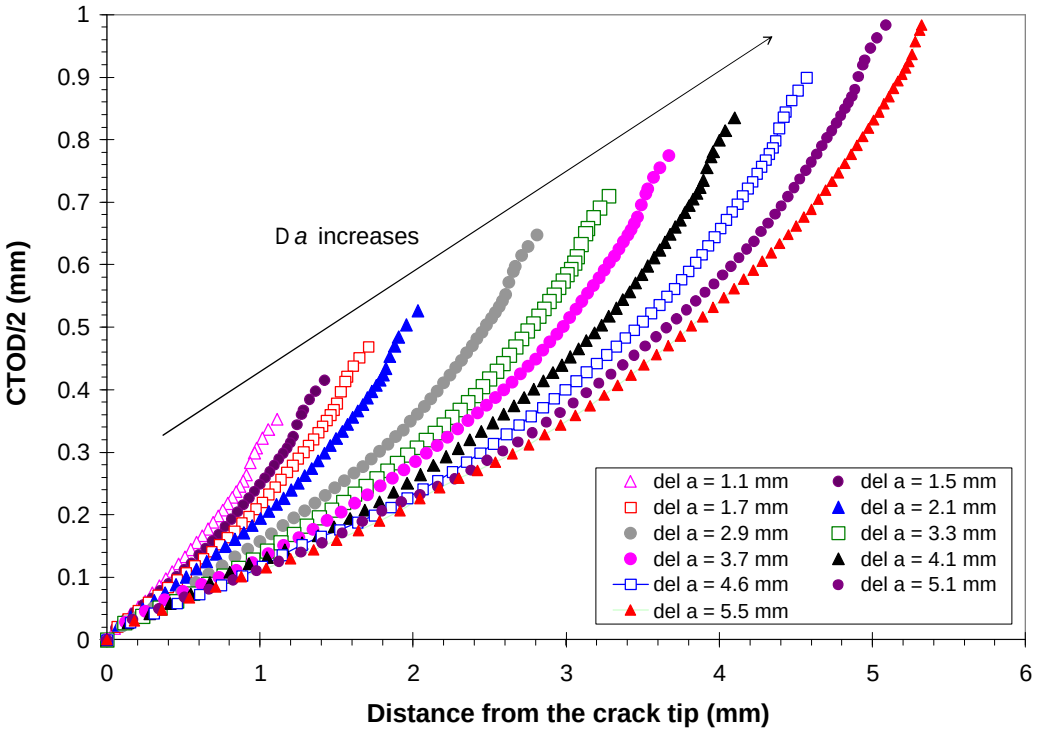

Figure 8 Comparison of the crack opening profiles calculated with 3D-FEA at the mid-plate of the SENB specimen

4. Two-Dimensional Finite Element Analyses

In previous section the 3D-FEA result of a growing crack (a/W= 0.59) was presented. The crack growth calculation is governed by the experimental data of crack extension vs. load point displacement (Fig. 4). Some of the 2D-FEA results of CTOD/CTOA are included in Figures 6 and 7 to demonstrate the adequacy of plane strain solution for this type of specimen configuration and loading. In particular, it has been shown that the feature of non-constant CTOD/CTOA in the early stage of crack growth is a common result for both two- and three-dimensional analyses, even when the crack tunneling effect is absent (experimentally and numerically). This feature is not a local phenomenon and is regardless of the location of measurement along the crack front across the specimen thickness.

Based on the results of the three- and two-dimensional analyses, it can be concluded that the stress state of these SENB specimens is predominantly plane strain. Therefore, the rest of the paper is focused on 2D-FEA. The specimen with a/W= 0.59 is analyzed first. This finite element model contains 13072 four-node reduced integration plane strain elements with 13635 nodes. Very fine mesh with square elements is populated in the potential crack growth region which extends to the edge of the specimen in order to facilitate the J-integral evaluation under potentially large scale yielding and extensive crack growth. The same material properties as shown in Figure 1 are used. The numerical analysis consists of two parts. The goal of the first part of the analysis is to

determine the CTOD/CTOA as a function of crack growth (Δa), based on the experimental input of crack extension vs. load point displacement curve. The second part of analysis is to evaluate the performance of the CTOD/CTOA fracture criteria based on the CTOD/CTOA values calculated from the first part of analysis.

The first part of analysis (for a/W= 0.59) follows exactly the same procedure as described previously in the case of 3D-FEA (Section 3). To verify the result, the predicted load-displacement curve is compared with the experimental data. Very good agreement was achieved and the result is similar to that presented in Figure 5. In addition, the predicted J-R curve can be reproduced within the experimental errors. The comparison will be shown in Section 6 together with the predictions for the other two SENB specimens (a/W= 0.32 and 0.71).

During the process of J-integral evaluation, the path dependency becomes noticeable as the amount of crack growth increases. The loss of the J-controlled crack growth may be related to the possible unloading behind the growing crack tip and the reverse yielding on the crack flanges [25,27-30]. Therefore, the J-values obtained from the outermost contour in the finite element model are used to compare with the ASTM-based experimental J-R curves [32]. This outer-most J-evaluation contour coincides with or close to the specimen boundary and is around the current crack tip [40,41].

5. CTOD/CTOA Fracture Criteria

As mentioned in the previous section, the first part of 2D-FEA allows the calculation for CTOD/CTOA by the given experimental data of crack extension vs. load point displacement. The CTOD values for a/W= 0.59 measured at 0.25, 0.5, and 1.0 mm behind the current crack tip are plotted in Figure 9. It can be seen that the initial CTOD values are relatively high and then progressively decrease to a nearly constant value. As a result, two CTOD/CTOA criteria may be proposed:

1. Constant CTOD/CTOA Criterion

The initially non-constant values of CTOD/CTOA are ignored. This is a popular approach which uses the constant part of CTOD/CTOA as a fracture criterion because the non-constant part is associated only with very small crack extension. In this particular case for a/W= 0.59, the crack growth is predicted with the finite element method and CTOD= 0.062 mm (see Fig. 9, which is obtained at 0.25 mm behind the crack tip in the first part of analysis – the determination of CTOD/CTOA in Section 4).

2 Bilinear CTOD/CTOA Criterion

For demonstration purpose, a bilinear form of the fracture criterion is used. As the dashed lines shown in Figure 9, the initial, non-constant values of CTOD/CTOA are taken into consideration. The first few data points for CTOD measured at 0.25 mm behind the crack tip are arbitrarily chosen for least-square fitting, which gives CTOD= 0.24 mm at zero crack growth and CTOD= 0.062 mm when Δa= 1.74 mm. The constant CTOD (0.062 mm) is assumed when Δa • 1.74 mm.

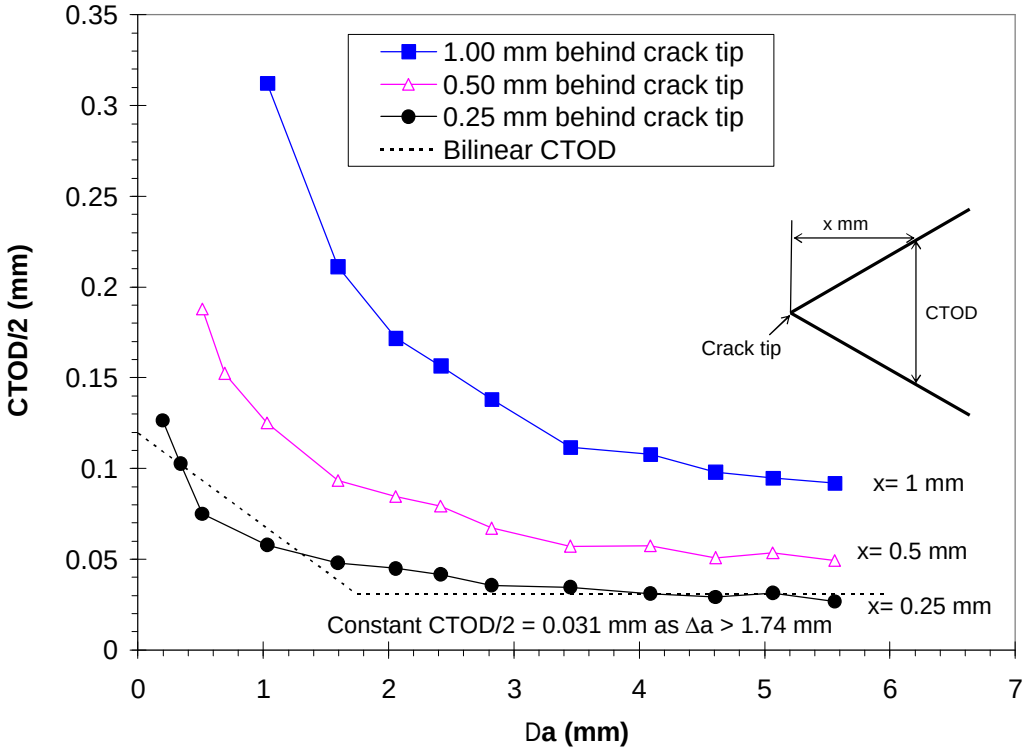

Figure 9 Calculated CTOD vs. crack extension for a/W = 0.59

As discussed earlier, the second part of the numerical analysis involves the prediction of crack growth with a given CTOD/CTOA criterion. With a constant CTOD fracture criterion (CTOD= 0.062 mm at 0.25 mm behind the current crack tip) and the ABAQUS [38] crack growth algorithm, the predicted load-displacement curve and the J-R curve are compared with the experimental data in Figures 10 and 11, respectively. It can be seen that this fracture criterion suffers a severe underestimation of the crack growth behavior. On the other hand, if the initial higher value of CTOD/CTOA is taken into consideration by using a simplified bilinear fracture criterion (Figure 9, dashed lines), the load-displacement and J-R curve can be recovered as shown in Figures 10 and 11. In fact, even with this simple bilinear fracture model, the prediction for the case of a/W= 0.59 works extremely well. Note that in this set of calculation, the CTOD/CTOA criterion is referenced at 0.25 mm behind the current crack tip. If the criterion is given at another location from the crack tip (say, 1 mm), it is expected that the same conclusion can be made, that is, without the initially higher values of CTOD/CTOA, the crack growth prediction will be underestimated. Note that in the current analysis, the non-constant feature of CTOD/CTOA is not a result of crack tunneling on the fracture surface of the specimen.

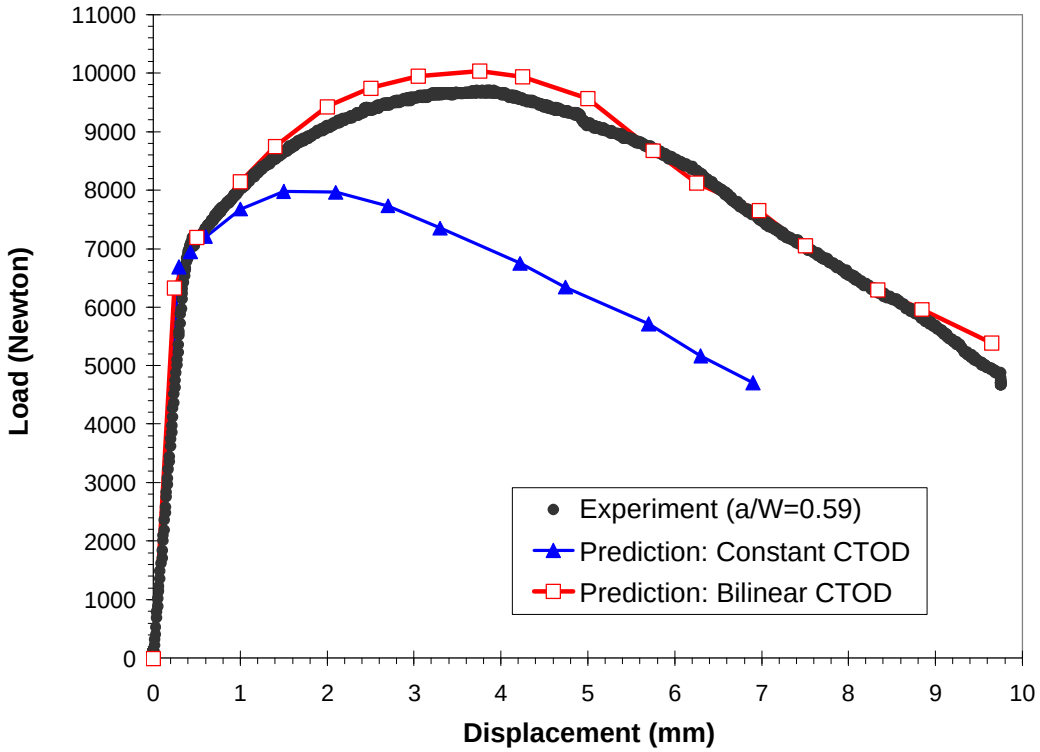

Figure 10 Comparison of predicted and experimental load-displacement curves for a/W= 0.59

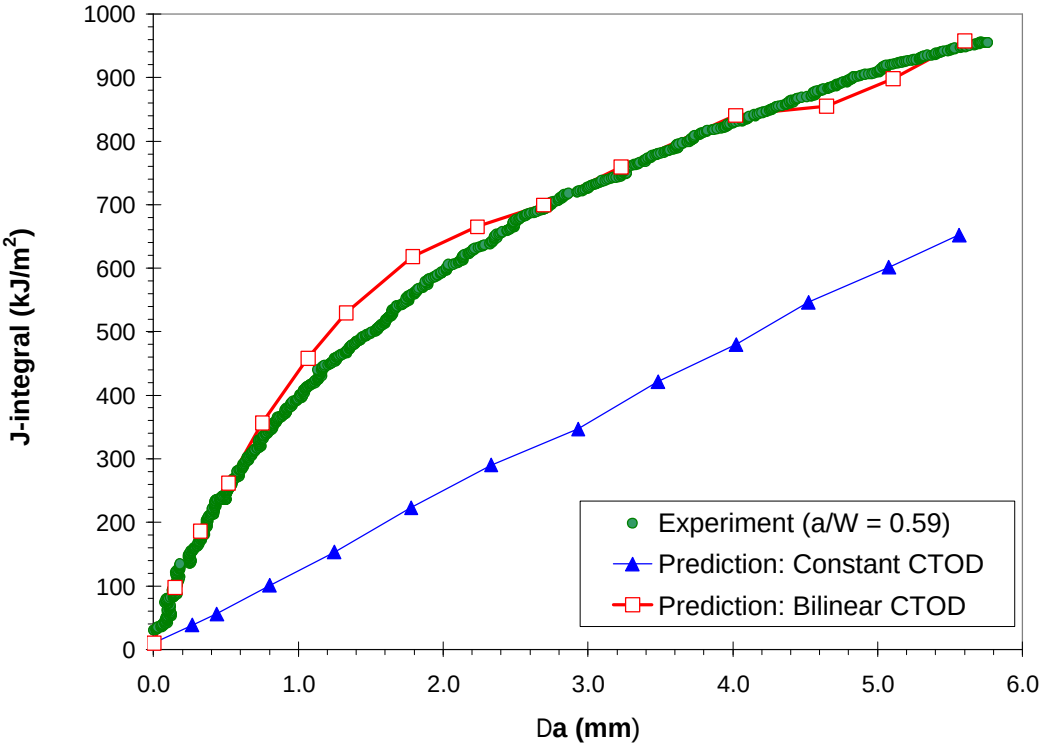

Figure 11 Comparison of predicted and experimental J-R curves for a/W= 0.59

6. Non-Constant CTOD/CTOA and Constraint Effect

The issue of the non-constant CTOD/CTOA is investigated in the context of crack tip constraint. Similar to the approach for the case of a/W =0.59, additional finite element analyses are performed for a high constraint specimen (a/W= 0.71) and for a low constraint specimen (a/W= 0.32). The J-R curves of these specimens (Fig. 3) clearly show the crack tip constraint effect, and the material (A285 carbon steel) is capable of sustaining a large amount of stable crack growth. The post-test fractography indicated that, similar to Figure 2, the crack fronts are relatively straight for these specimens. Based on the results of 3D/2D-FEA for the case of a/W=0.59, only plane strain analyses are performed for these two additional configurations.

6.1. Effect of Constraint on J-R Curve and CTOD/CTOA

The finite element model for the high constraint specimen (a/W= 0.71) contains 13078 four-node elements with 13647 nodes. Similar model was designed for the low constraint case (a/W= 0.32) which has 13070 elements and 13631 nodes. Very fine, square mesh is placed around the crack tip and extends to the specimen edges for proper crack growth simulation and J-integral evaluation. The experimental curve of load-point displacement versus crack extension for each specimen is used as the fracture criterion to simulate crack growth and to calculate CTOD/CTOA. As a result, the finite element calculated J-R curves (open symbols in Fig. 12) are plotted against the experimental data points in Figure 12. The good agreement again shows the adequacy of plane strain assumption and the numerical scheme. The constraint effect is obviously reflected by these J-R curves for a/W= 0.32, 0.59, and 0.71, respectively.

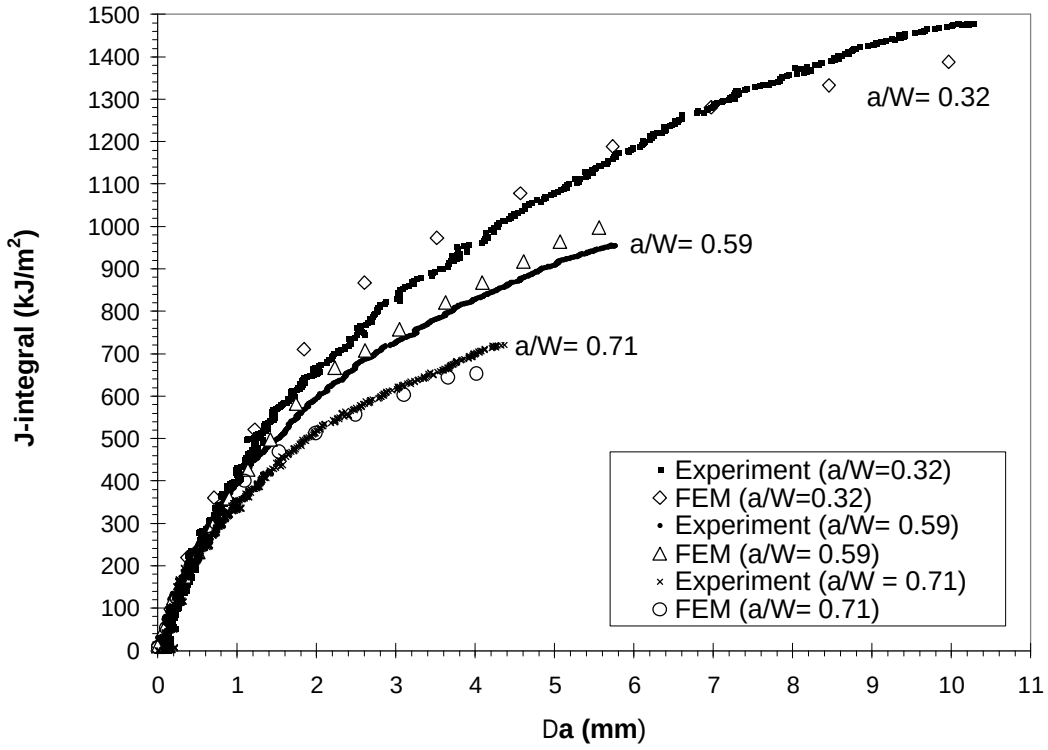

Figure 12 Comparison of predicted and experimental J-R curves

The associated CTOA values are calculated for these three specimens at a fixed distance of 1 mm behind the current crack tip. In Figure 13, it appears that each CTOA vs. Δa curve eventually approaches to a specific, but different, constant value. Apparently, these CTOA curves are functions of a/W, that is, crack tip constraint.

The importance of the initial, higher values of CTOD/CTOA has been demonstrated in Figures 10 and 11. Without taking consideration of non-constant portion of the fracture criterion, it would be detrimental for the subsequent prediction of crack growth. Attempts were made to use the bilinear CTOD/CTOA criterion based on the case of a/W= 0.59 (Fig. 9) to predict the crack growth behavior for the cases of a/W=0.32 and 0.71, respectively. However, the prediction tends to overestimate the experimental data, although the results are superior to those obtained with a constant CTOD/CTOA fracture criterion. Again, this implies that the CTOD/CTOA is indeed constraint-dependent.

One of the objectives of this paper is to emphasize the necessity to include the initial values of CTOD/CTOA in formulating a fracture criterion. A simple bilinear form has shown its viability in crack growth prediction for the case of a/W= 0.59. Therefore, the same demonstration will not be repeated for the cases of a/W= 0.71 and 0.32. In conjunction with Figures 3, 12, and 13, there is a clear connection between the crack tip constraint and the CTOD/CTOA fracture criteria. For further improvement in predicting crack growth, a more sophisticated fracture criterion should be developed to include the constraint effect.

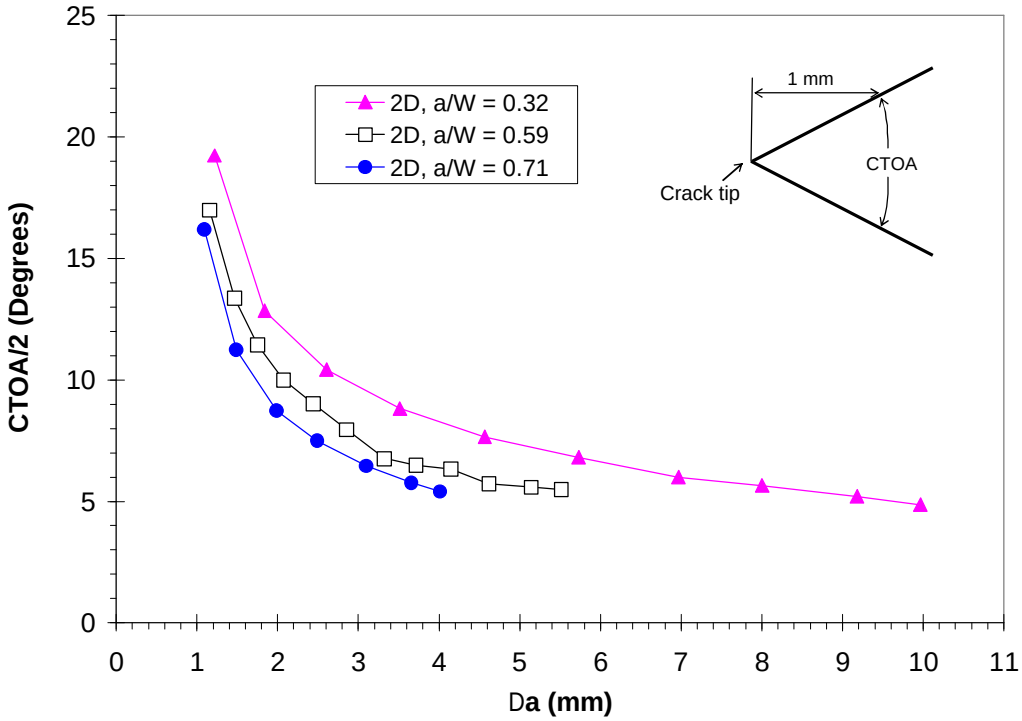

Fig.13 Comparison of CTOA for SENB specimens with various crack tip constraint level

6.2. Theoretical Prediction of CTOD/CTOA

Using the Dougdale-Barenblatt strip yield model, the J-integral evaluation which utilizes the crack tip field solved by complex variable methods will lead to a simple expression between J and CTOD (δ_t):

$$J = \sigma_y \delta_t \qquad (1)$$

where σ_y is a "generic" yield stress (as opposed to the 0.2% offset yield stress, σ_o). On the other hand, for a power law material characterized by Hutchinson-Rice-Rosengren (HRR) solution, and to define δ_t as the crack opening displacement between the intercepts of the two symmetric ±45° lines emanating from the deformed crack tip and the crack flange profile, it can be shown (e.g., [37]) that

$$J = \sigma_y \delta_t / d_n \qquad (2)$$

where d_n has been calculated by Shih [44] for cases of plane strain and plane stress, and is sown to be a strong function of strain hardening exponent (n) but weakly dependent of σ_y/E. For most of the engineering materials, $0 < d_n \bullet 1$ for plane stress and $0 < d_n < 0.8$ for plane strain [37,44]. From Eq. (1) and more generally on Eq. (2), Kanninen et al. [37] pointed out that J and δ_t , or CTOD, is equivalent, and "any fracture criterion based upon

a critical value of δ_t is equivalent to one based upon a critical value of J and vise versa." Of course, the HRR dominance must be satisfied in this aspect.

Combining Eqs. (1) and (2), J may be expressed as [17,42]

$$J = m\sigma_y \delta_t \quad (3)$$

where m may be a constant for a specific material. By differentiation of Eq. (3) with respect to the crack length (a), with an additional approximation that m remains unchanged during (limited amount of) crack extension, then the relationship between CTOA and the slope of the J-R curve (or tearing modulus) may be established [17,43]:

$$CTOA = d\delta_t/da = (dJ/da)/(m\sigma_y) \quad (4)$$

It appears that the factor m can be obtained by experimental data if J-R curve is known and CTOA has been calculated or measured. However, practically speaking, the factor m may not be exactly a constant due to the fluctuation of the experimental data points, and it may somehow depend on the crack tip constraint. For demonstration purpose, the value of m is solved by using the first data point in Figure 13 and the experimental J-R curve for each specimen.

Because Eq. 4 is very sensitive to the local slope if the full set of experimental data is used, each experimental J-R curve in Figure 3 or 12 is first fit with a forth-order polynomial using data points at every 0.5 mm increment of crack growth. To take strain hardening into consideration, the flow stress of this material (σ_f= 333 MPa) is used in place of σ_y. The values of m derived from this process are 1.254, 1.208, and 1.059, respectively, for specimens with a/W of 0.32, 0.59, and 0.71. The predicted CTOA as a function of Δa can be seen in Figure 14, on which the data points used in Figure 13 are superimposed for comparison. A qualitative agreement is achieved between the finite element-calculated CTOA and the prediction based on experimental J-R curves. Therefore, the initially higher values of CTOD/CTOA are indeed a natural consequence of the crack growth resistance.

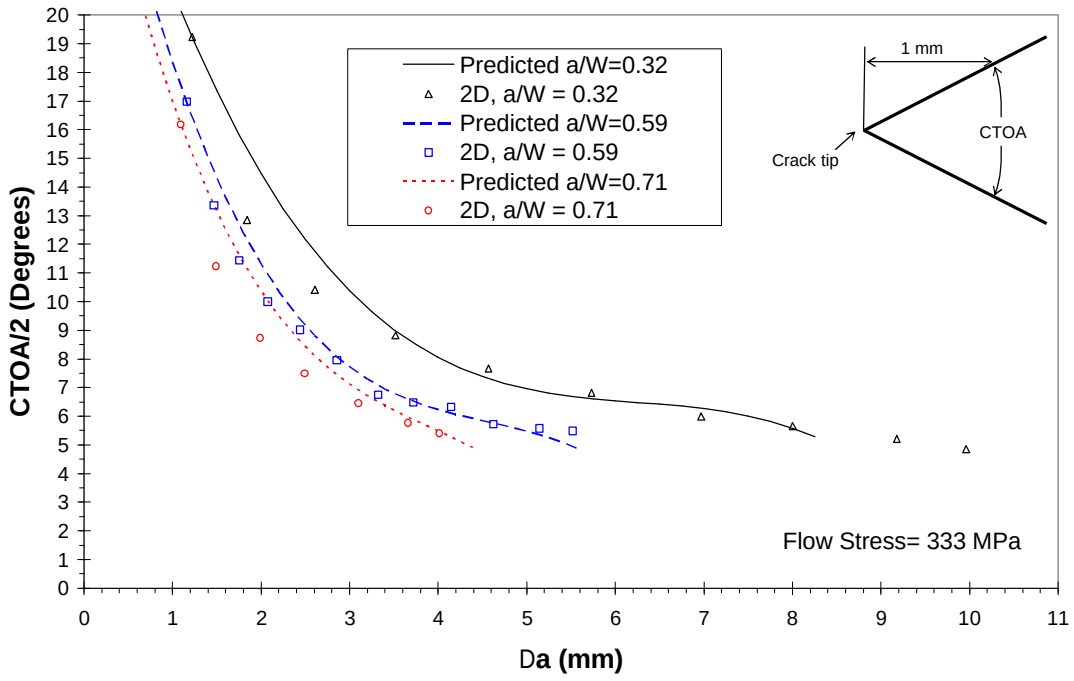

Figure 14 Theoretical prediction of CTOA based on J-R curves

7. Conclusions and Discussions

The J-integral experimental data obtained from SENB specimens with various degrees of crack tip constraint are used to investigate a suitable description for CTOD/CTOA fracture criteria. The fractography of the post-test specimens showed that the crack fronts are straight. Therefore, the crack tunneling is eliminated as an influential factor in this study. Both three- and two-dimensional finite element analyses are performed to simulate the ASTM E 1820 J-integral testing. The similarity of these finite element solutions confirms that the deformation is essentially plane strain, and the two-dimensional analysis is adequate for the determination of CTOD/CTOA during the crack growth. Consequently, the plane strain analysis is employed and is combined with the CTOD/CTOA fracture criteria to conversely predict the J-integral testing so the performance of these fracture criteria can be evaluated.

During the process of simulating crack growth, the crack tip nodes are gradually released according to the experimental data (crack extension vs. load-point displacement curve, e.g., Fig. 4). The CTOD/CTOA at each increment of crack extension can be calculated at a fixed distance from the current crack tip. Figure 15 shows the current result (a/W= 0.59) plotted with the literature data [7-11], which were originally collected and presented by Newman et al. [6]. A common feature of these data sets sampled in Figure 15 is the higher CTOD/CTOA values in the early stage of crack growth. After a small amount of crack growth, each data set decreases progressively to a relatively constant value.

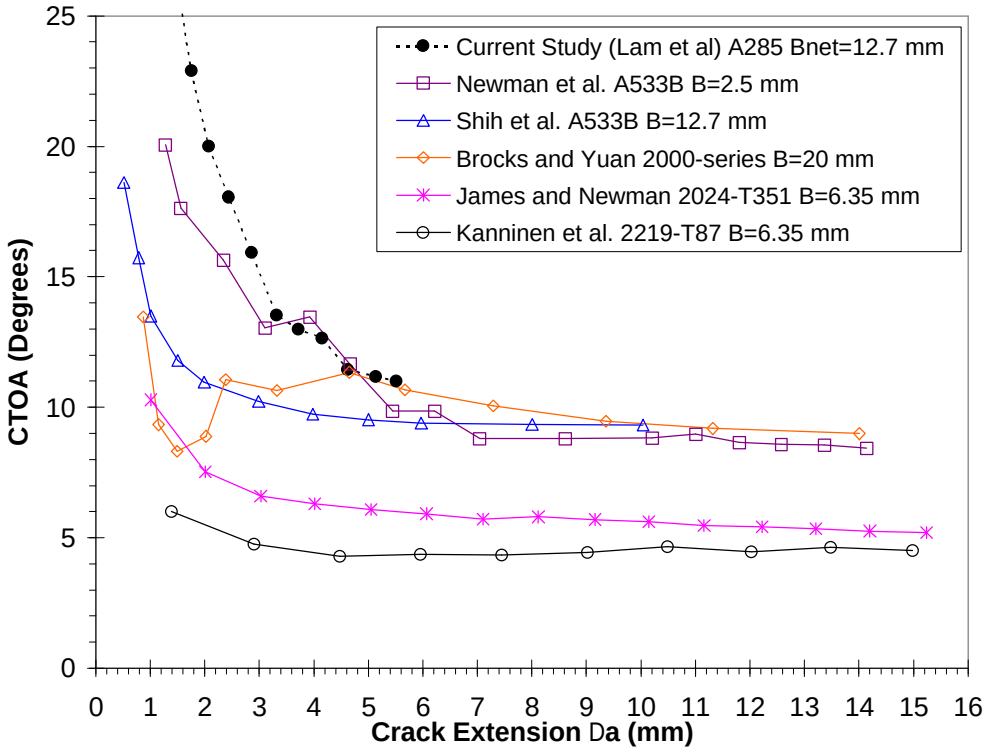

Figure 15 Typical literature data of COTA (reproduced from Reference 6) and the current result

Newman et al. [6] suggested that constraint effect and the crack tunneling may be the key issues to explain why the "constant" CTOD/CTOA criterion works so well. Based on their work on mostly thin aluminum specimens, they concluded that the concept of a constant CTOD/CTOA can be supported, provided that the crack length to thickness ratio and the uncracked ligament to thickness ratio are no less than 4. They speculated that the non-constant CTOD/CTOA may be attributed by the assumption of inappropriate stress state (i.e., two-dimensional analyses) and by severe crack tunneling. However, the current research has eliminated the presence of crack tunneling, and yet both 2D- and 3D-FEA show the same phenomenon of the initially high CTOD/CTOA for these carbon steel, side-grooved specimens with a net thickness of 12.7 mm (0.5 in.). In addition, it has been shown that a relationship can be established between the CTOD/CTOA and the J-integral/tearing modulus, at least for power law (HRR) materials [36,37,43] and for the perfectly plastic materials [17,42]. This relationship will analytically lead to higher CTOD/CTOA values in the beginning of crack growth, and then progressively decrease to a nearly constant value for most of the materials that exhibit typical J-R curves.

The condition of in-plane constraint seems to provide a reasonable explanation for the success of the constant CTOD/CTOA fracture criterion as applied to thinner specimens.

As pointed out by Chao [45], under plane stress conditions a single fracture parameter is sufficient to describe the crack tip stress and strain fields for wide variety of test specimens. Therefore, the constraint effect in fracture mechanics is negligible in the case of plane stress specimens. As a result, the CTOD/CTOA fracture criterion is capable of predicting long range stable crack growth under plane stress, which in aluminum sheets it is not uncommon that Δa exceeds 50 mm. Unlike in the case of plane strain or thick specimens, additional parameter is needed to fully characterize the near crack tip fields, such as the J-A_2 three-term solution [33-35]. In this case the J-R curve is a function of specimen geometry, for example, the crack depth or a/w, as seen in Figure 3. In the same token, if the CTOD/CTOA fracture criterion is to be used, it must also depend on the specimen configuration (see Figure 13).

The initially higher values of CTOD/CTOA are likely related to the transition from crack blunting to stable crack growth. This phenomenon exists for both plane strain and plane stress specimens (Fig. 15). As shown in Section 5, this initial CTOD/CTOA is important in predicting crack growth in specimens under predominantly plane strain conditions. This implies that the initial part of CTOD/CTOA is strongly dependent of crack tip constraint, and without considering the initial values, the crack growth behavior is severely underestimated (Figs. 10,11). Since the constraint effect in the plane stress type of specimens is insignificant [45], it then can be concluded that the initial part of CTOD/CTOA may be negligible in the formulation of fracture criteria for this type of stress state. Therefore, the proposed approach of a "constant" CTOD/CTOA fracture criterion (e.g., Newman et al. [6]) for specimens such as thin aluminum sheets may still be theoretically sound.

Unfortunately, the functional dependence between the CTOD/CTOA and the constraint parameter such as A_2 [33-35], T [46], or Q [47,48], has not been well established. The key to overcome this difficulty seems to rely on the development of a complete solution which, in particular, must be valid in the area immediately behind the advancing crack tip where unloading is known to occur [25-30].

Acknowledgment

The fracture testing performed by G. K. Chapman and Dr. M. J. Morgan of Savannah River National Laboratory (SRNL) is greatly appreciated. PSL acknowledges the support from the United States Department of Energy (DOE) Office of Science Environmental Management Science Program (EMSP), and from SRNL/Savannah River Site (SRS) High Level Waste Division under the Independent R&D Program, funded by DOE under Contract No. DE-AC09-96SR18500. YK and YJC were supported by the U. S. National Science Foundation grant CMS0116238 and partially by DOE through the South Carolina Universities Research and Education Foundation (SCUREF).

References

[1] Mahmoud S, Lease K. The effect of specimen thickness on the characterization of critical CTOA in 2024-T351 aluminum alloy, Engng Fract Mech 2003;70:443-56.

[2] Luo PF, Chao YJ, Sutton MA, Application of stereo vision to 3D deformation analysis in fracture mechanics, Optical Engineering 1994;33(3):981-990.
[3] Chao YJ, Sutton MA. Accurate measurement of two- and three-dimensional surface deformations for fracture specimens by computer vision: Experimental Techniques in Fracture; ed. Epstein JS, VCH Publisher 1993;59-94.
[4] Lloyd WR. Microtopography for ductile fracture process characterization: Part 1: Theory and methodology, Engng Fract Mech 2003;70:387-401.
[5] Newman Jr JC, Zerbst U. Engineering fracture mechanics. Engng Fract Mech 2003;70:367-69
[6] Newman Jr JC, James MA, Zerbst U. A review of the CTOA/CTOD fracture criterion. Engng Fract Mech 2003;70:371-85
[7] Shih CF, de Lorenzi HG, Andrews WR. Studies on crack initiation and stable crack growth. ASTM STP 1979;668:65–120.
[8] Kanninen MF, Rybicki EF, Stonesifer RB, Broek D, Rosenfield AR, Nalin GT. Elastic–plastic fracture mechanics for two dimensional stable crack growth and instability problems. ASTM STP 1979;668:121–50.
[9] Brocks W, Yuan H. Numerical studies on stable crack growth. In: Defect Assessment in Components Fundamentals and Applications, vol. 9. ESIS Publication; 1991:19–33.
[10] Newman Jr JC, Shivakumar KN, McCabe DE. Finite element fracture simulation of A533B steel sheet specimens. In: Defect Assessment in Components Fundamentals and Applications, 9. ESIS Publication; 1991:117–26.
[11] James MA, Newman Jr JC. Three-dimensional analyses of crack-tip-opening angles and δ5-resistance curves for 2024-T351 aluminum alloy. ASTM STP 2002;1406:279–97.
[12] Newman Jr JC, Booth BC, Shivakumar KN. An elastic–plastic finite-element analysis of the J-resistance curve using a CTOD criterion. ASTM STP 1988;945:665–85.
[13] Newman Jr JC, Dawicke DS, Bigelow CA. Finite-element analyses and fracture simulation in thin-sheet aluminum alloy. In: Durability of Metal Aircraft Structures. Georgia: W.H. Wolfe Associates; 1992:167–86.
[14] Dawicke DS, Sutton MA. CTOA and crack tunneling measurements in thin sheet 2024-T3 aluminum alloy. Exp Mech 1994;34(4):357.
[15] Dawicke DS, Piascik RS, Newman JC, Jr. Analysis of stable tearing in a 7.6 mm thick aluminum plate alloy, Fatigue and Fracture Mechanics: 28th Volume, *ASTM STP 1321*, American Society for Testing and Materials 1997:309-324.
[16] Dawicke DS, Sutton MA, Newman Jr JC, Bigelow CA. Measurement and analysis of critical CTOA for an aluminum alloy sheet. ASTM STP 1999;1220:358–79.
[17] Gullerud AS, Dodds Jr RH, Hampton RW, Dawicke DS. Three-dimensional modeling of ductile crack growth in thin sheet metals: computational aspects and validation. Engng Fract Mech 1999;63:347–74.
[18] Hampton RW, Nelson D, Stable crack growth and instability prediction in thin plates and cylinders. Engng Frac Mech 2003:469-491.
[19] Mahmoud S, Lease K. Two-dimensional and three-dimensional finite element analysis of critical crack-tip-opening angle in 2024-T351 aluminum alloy at four thicknesses. Engng Fract Mech 2004;71:1379-91.

[20] Shterenlikht A, Hashemi SH, Howard IC, Yates JR, Andrews RM, A specimen for studying the resistance to ductile crack propagation in pipes, Engng Frac Mech 2004;71:1997-2013.
[21] Shivakumar KN, Newman Jr JC. ZIP3D—An elastic and elastic–plastic finite-element analysis program for cracked bodies, NASA TM 102753, 1990.
[22] James MA, Residual strength calculations for single and multiple-site damage cracks. First Joint DoD/FAA/NASA Conference on Aging Aircraft, July 1997;1789–802.
[23] James MA, Newman Jr JC. Importance of crack tunneling during fracture: experiments and CTOA analyses, 10th International Congress of Fracture, Honolulu, Hawaii, December 3–7, 2001.
[24] Koppenhoefer KC, Gullerud AS, Ruggieri C, Dodds Jr RH. WARP3D: Dynamic nonlinear analysis of solids using a preconditioned conjugate gradient software architecture, Structural Research Series 596, UILU-ENG-94-2017, University of Illinois, 1994.
[25] Rice JR, Drugan WJ, Sham TL. Elastic-plastic of growing cracks. ASTM STP 1980;700:189-221.
[26] Dean R, Hutchinson JW. Quasi-static steady crack growth in small scale yielding, ASTM 1980;700:383-405.
[27] Parks DM, Lam PS, McMeeking RM. Some effects on inelastic constitutive models on crack tip fields in steady quasistatic growth. Advances in Fracture Research 1981; 5:2607-14.
[28] Lam PS. Numerical analysis of stable crack growth in elastic-plastic materials in small scale and general yielding. UILU-ENG 82-6003 1982; Univ. of Illinois T&AM Report No. 455.
[29] Lam PS, McMeeking RM. Analysis of steady state quasistatic crack growth in plane strain tension in elastic-plastic materials with non-isotropic hardening. J Mech Phys Solids 1984;32: 395-414.
[30] Lam PS, Freund LB. Analysis of dynamic growth of a tensile crack in an elastic-plastic material. J Mech Phys Solids 1985;33: 153-67.
[31] Hermann L, Rice JR. Comparison of experiment and theory for elastic-plastic plane strain crack growth. Metal Science 1980: 285-91.
[32] Lam PS, Chao YJ, Zhu XK, Kim Y, Sindelar RL. Determination of Constraint-Modified J-R Curves for Carbon Steel Tanks. J Press Vessel Tech 2003;125:136-43.
[33] Yang S, Chao YJ, Sutton MA. Higher order asymptotic crack tip fields in a power-law hardening material. Engng Fract Mech 1993;45:1-20.
[34] Yang S, Chao YJ, Sutton MA., Complete theoretical analysis for higher order asymptotic terms and the HRR zone at a crack tip for mode I and Mode II loading of a hardening material. ACTA MECHANICA 1993;98:79-98.
[35] Chao YJ, Yang S, Sutton MA. On the fracture of solids characterized by one or two parameters: theory and practice. J Mech Phys Solids 1994;42:629-47.
[36] Kanninen MF et al. Development of a Plastic Fracture Methodology. EPRI NP-1734, Project 601-1, Final Report, March 1981.
[37] Kanninen MF, Popelar CH. Advanced Fracture Mechanics. Oxford University Press 1985.
[38] ABAQUS Standard, ABAQUS Inc., Pawtucket, RI.

[39] Lloyd WR, McClintock FA. Microtopography for ductile fracture process characterization: Part 2: Application for CTOA analysis, Engng Fract Mech 2003;70: 403-15.
[40] Moskovic R, O'Dowd N, Flewitt P. Experimental and numerical study of crack growth in the heat-affected-zone of a ferritic steel weldment. Transactions of the 17th conference on Structural Mechanics in Reactor Technology (SMiRT 17), Prague, Czech Republic August 17-22, 2003.
[41] O'Dowd N. Wylfa Superheater Headers Project : Numerical study of crack in welded joints, Imperial College London Report ME288, 2001.
[42] Anderson TL. Fracture Mechanics: Fundamentals and Applications 2nd Ed. CRC Press, 1995.
[43] Omidvar B, Wnuk M, Choroszynski, Relationship between the CTOD and the J-integral for stationary and growing cracks: Close form solutions, Int. J. Fract 1997; 87:331-43.
[44] Shih CF, Relationship between the J-integral and the crack displacement for stationary and extending cracks, J. Mech. Phys. Solids 1981:29:305-26.
[45] Chao YJ, On a single parameter controlled fracture of solids under plane stress conditions, Int. J. Fract. 1993; 62:R7-R10.
[46] Betegon C, Hancock JW. Two parameter characterization of elastic-plastic crack-tip fields, J. Appl. Mech. 1991; 58:104–10.
[47] O'Dowd NP, Shih CF. Family of crack-tip fields characterized by a triaxiality parameter - I. Structure of fields, J. Mech. Phys. Solids 1991;39:989–1015.
[48] O'Dowd NP, Shih CF. Family of crack-tip fields characterized by a triaxiality parameter - II. Fracture applications, J. Mech. Phys. Solids 1992; 40:939–63.